Detection and Correction of Ectopic Beats for HRV Analysis Applying Discrete Wavelet Transforms

Desmond B. Keenan

Abstract—The clinical usefulness of heart rate variability is limited to the range of Holter monitoring software available. These software algorithms require a normal sinus rhythm to accurately acquire heart rate variability (HRV) measures in the frequency domain. Premature ventricular contractions (PVC) or more commonly referred to as ectopic beats, frequent in heart failure, hinder this analysis and introduce ambiguity. This investigation demonstrates an algorithm to automatically detect ectopic beats by analyzing discrete wavelet transform coefficients. Two techniques for filtering and replacing the ectopic beats from the RR signal are compared. One technique applies wavelet hard thresholding techniques and another applies linear interpolation to replace ectopic cycles. The results demonstrate through simulation, and signals acquired from a 24hr ambulatory recorder, that these techniques can accurately detect PVC's and remove the noise and leakage effects produced by ectopic cycles retaining smooth spectra with the minimum of error.

Keywords—Heart rate variability, vagal tone, sympathetic, parasympathetic, wavelets, ectopic beats, spectral analysis.

I. INTRODUCTION

HEART rate variability is a measure of alterations in heart rate by measuring the variation of RR intervals and has been shown to provide an assessment of cardiovascular disease [1]. Heart rate is influenced by both sympathetic and parasympathetic (vagal) activity. The influence and balance of both branches of the anatomic nervous system (ANS) is known as sympathovagal tone reflected in the RR interval changes. HRV measurements can be made by spectral analysis where a measure of the power in each of four frequency bands is representative of the four components of HRV. A low frequency (LF) component provides a measure of sympathetic effects on the heart and generally occurs in a band between 0.04 Hz and 0.15 Hz. Non regular effects such as chemoreceptors, thermoreceptors, and the reninangiothensin system can be monitored at ultra-low frequencies. A measurement of the influence of the vagus nerve in modulating the sinoatrial node can be made in the high frequency band (HF) loosely defined between 0.15 and 0.4 Hz known as respiratory sinus arrhythmia (RSA), and is a

D. B. Keenan is with Research and Development, Medtronic MiniMed, Northridge, CA 91325 USA (phone: 818-576-4472; fax: 818-576-6206; e-mail: barry.keenan@ medtronic.com).

measure of cardiac parasympathetic activity. This rhythm is generated by the sinoatrial node; sometimes referred to as the pacemaker of the heart, and is nodal tissue located on the upper wall of the right atrium and sets the rate of contraction by generating nerve impulses causing the atria to contract. This frequency band or rate of contractions can be variable though closely related to the frequency of respiration. The ratio of power in the LF and HF bands (LF/HF) provides a measure of cardiac sympathovagal balance. Several studies have indicated that the powers of the LF and HF components, occurring in synchrony with vasomotor waves and respiratory acts, respectively, appear to reflect in their reciprocal relationship the state of sympathovagal balance in numerous physiological and pathophysiological conditions [2-4]. A correlation between body fat content and the LF/HF ratio after glucose ingestion have been correlated in nonobese subjects with various levels of body fat content [5]. Decreased values of HRV measures are indirectly proportional to pressure, body mass index and insulinemia in young and obese patients without clinical symptoms of cardiovascular disease, diabetes or damage of target organs. In a study by Ravagli et al [6], pressure values correlated closely with the insulin level. These HRV measurements in the simplest form can be sensitive to stress i.e. the mental load on the brain. This measure can be seen to decrease with age, which has been attributed to a decrease in efferent vagal tone. Exercise on the other hand increases vagal tone. The scope of what HRV is capable of diagnosing or determining is far from understood and it is a busy area of research. It has been used as a measure of mortality primarily with patients who have undergone cardiac surgery. Clinical depression strongly associated with mortality with such patients may be seen through a decrease in HRV [7]. Spectral HRV was previously described as a measure of power in various frequency bands. To determine the RSA amplitude over a period of time, frequency domain, time domain and phase domain approaches have been analyzed. A time-domain approach by Grossman [8] known as the peak-valley algorithm measures the maxima and minima values of RR time intervals within each breath. In the frequency domain a value for RSA can be derived by applying an appropriate window function to a given time series to reduce spectral leakage from random events and applying the Fourier transform to the filter residuals. When analyzing the HF band

the respiratory frequency should be predetermined through some kind of respiratory monitor, determined through paced breathing or at worst estimated. This frequency domain approach takes the average response over time, nominally a 5-minute period. This approach provides little information about the RSA waveform as it is time averaged and may not reflect the cardiac vagal dynamics. Another approach to evaluating RSA has been to analyze dynamics of heart rate with respect to phase [9] and is referred to as the phase domain approach. Frequency domain approaches to HRV, which are essential for the low frequency sympathetic measures are greatly hindered by the presence of ectopic beats [10-11]. Ectopic beats, when activated in the ventricles, are fairly common in subjects suffering from heart failure. There exist algorithms that detect and classify ectopic beats [12], but for HRV analysis these beats must be removed either by editing [13], or some means of interpolation or filtering. This paper describes a wavelet-based approach using Daubechies wavelets for detecting and filtering PVCs, and compares the filtering technique to linear interpolation based on simulation data and data from a heart failure patient.

II. METHODS

A. Data Collection

The data in this investigation was collected from an ambulatory monitoring device, the LifeShirt. The LifeShirt employs the Konno and Mead [14] two compartment-breathing model of the respiratory system. This approach shows changes in tidal volume measured at the mouth to be comparable to the sum of changes in ribcage and abdominal contributions. These volume changes are normally obtained by measuring variations in the thoracic and abdominal regions by inductive plethysmography (IP), magnetometers, or strain gauges [15-17]. The LifeShirt contains two IP sensors encircling the ribcage and abdomen used to measure tidal volume. A low oscillating current is passed through these inductive bands creating a magnetic field that is required to measure the self-inductance of the band's coil. The self-inductance of the coil is proportional to the cross sectional area of the band. As this cross sectional area changes the coils self-inductance changes. Changes in self-inductance are measured by integrating an oscillator circuit whose resonant frequency varies with changes in self-inductance. A counter measures this resonant frequency by counting the pulses produced by the oscillator over time, creating a waveform proportional to changes in the cross sectional area. These bands are then calibrated to adjust the contribution of each band to overall tidal volume base on Equation (1)

$$Vt = k.RC + l.AB \qquad (1)$$

where Vt is the tidal volume measurement, RC and AB are the ribcage and abdominal bands, and k and l are calibration coefficients that apply the appropriate gain to each signal based on a calibration algorithm [18][19]. The LifeShirt

acquires single lead ECG (lead II) sampled at a rate of 200 Hz, which is linearly interpolated in software by a factor of 5, producing an ECG with 1 kHz resolution. Heart rate is determined based on the Pan-Tompkins algorithm [20] for QRS detection. The RR interval signal is derived from the temporal R wave peak, which is determined by locating the peak point within the QRS complex. The RR signal is then processed by filters and uniformly sampled prior to spectral analysis.

B. Spectral Analysis

The instantaneous RR interval is preprocessed creating a uniformaly sampled signal. This process is illustrated in Figure 1 where the instantaneous RR interval is uniformly sampled at 50Hz and resampled at 5Hz by low pass filter decimation.
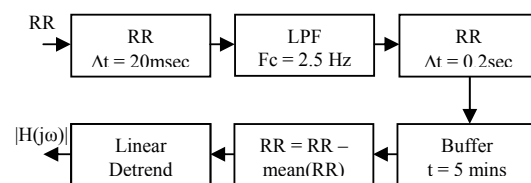

Fig. 1 Block diagram of HRV preprocessing

Five-minute time windows are detrended using a best straight line fit approach with the segment mean removed. Welch's [21] power spectral density estimation approach is then applied. Welch's averaged, modified periodogram method that applies sections of the RR signal with 50% overlap, with each section windowed with a Hamming window and nine modified periodograms are computed and averaged. A five-minute window is decomposed into 1-minute windows with 300 samples; sampled at 5 Hz. Each 1 minute window is zero padded to a 2048 sample length and the power of the FFT averaged. Various window functions may be applied, although a rectangular window will normally introduce some spectral leakage, and other window functions such as Blackman-Harris and Nutal can smear the spectra, but are also preferred in certain circumstances. The power in the LF and HF bands is determined [22] and the ratio of LF and HF calculated to evaluate sympatovagal balance.

C. Discrete Wavelet Transform

Prior to spectral analysis ectopic beats are identified and processed. The discrete wavelet transform (DWT) is used for both identification and filtering of ectopic beats. Wavelet coefficients at the highest level of detail are analyzed to locate the ectopic cycles. The DWT coefficients are obtained from the unprocessed RR interval signal by decomposing it into a set of frequency bands by applying low pass and high pass filter banks. Theses subbands are distributed logarithmically in frequency, each sampled at a rate that has a natural proportion to the frequencies in that band. Figure 2 illustrates this subband decomposition where the original signal x[n] or

in this case the instantaneous RR interval is passed through a halfband high pass filter h[n] and a low pass filter g[n] creating two subbands both sampled at half the original frequency.
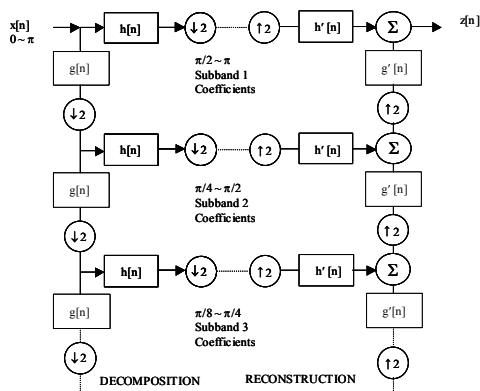

Fig. 2 Wavelet decomposition and reconstruction

These filters approximate halfband FIR filters that are determined by the choice of wavelet. The bandwidth of each filter output and subband is illustrated by a fraction of the sampling frequency where π is equal to the Nyquist rate or half the sampling frequency, therefore half of the samples can be eliminated. This demonstrates one level of wavelet decomposition, which can be expressed as:

$$y_h[k] = \sum_n x[n]h[2k-n] \qquad (2)$$

$$y_g[k] = \sum_n x[n]g[2k-n] \qquad (3)$$

where the g terms denote the low pass output and h terms denote the high pass output. This decomposition is reapplied to the low subband output repeatedly creating logarithmic resolution in the frequency domain. This has the effect of doubling the frequency resolution and reducing the time resolution by a factor of 2 since half the number of samples now make up the signal. This subband coding procedure is repeated for further decomposition until there is no data left to decompose, where every decomposition results in half the number of samples, thereby decreasing the time resolution by a factor of 2 and taking half the frequency band thereby doubling the frequency resolution. Only ideal halfband filters such as various wavelet packets allow for perfect reconstruction to the original signal, for example Daubechies set of wavelets [23]. Also illustrated in Figure 2 is the reconstruction process of this decomposed signal. Reconstruction normally takes places after some kind of soft or hard thresholding, or compression. The reconstruction in the case of wavelets uses the fact that these halfband filters form orthonormal bases. Therefore the decomposition procedure is followed in reverse order for the reconstruction. The wavelet subband coefficients at every level are upsampled by two, passed through synthesis filters g'[n], and h'[n] (high

pass and low pass) which make up the inverse discrete wavelet transform (iDWT), and are added. The analysis and synthesis filters are identical to each other, except for a time reversal. Signal reconstruction is therefore the inverse DWT. The reconstruction process is shown on the right side Figure 2. The signal is interpolated by filling in zeros for every other sample prior to filtering thereby restoring the subband of the signal to its original length. This process is expressed by Equation (4).

$$z[k] = \sum_b h'[n]y'[2k-n] + \sum_n g'[n]d[2k-n] \qquad (4)$$

D. Thresholding

Following decomposition and prior to the wavelet reconstruction process, ectopic beats are removed by a thresholding process. Soft thresholding or shrinkage requires selecting a threshold where all wavelet coefficients in each subband falling below this threshold are reduced to zero and coefficients above this thereshold have the threshold subtracted from it, so the coefficients tend toward zero. Hard thresholding requires reducing the coefficients below this threshold to zero leaving coefficients above this threshold constant. This nonlinear approach is very different from conventional filtering and has been shown to be very effective denoising images. Donoho and Johnstone [24-27] have demonstrated the usefulness of this approach against traditional linear methods of smoothing which suppress noise, but can also broaden the signals features, which can lead to error in HRV measures. This hard thresholding approach is demonstrated by Equation (5):

$$w[n] = \begin{cases} 0, & w[n] > T \\ w[n], & w[n] < T \end{cases} \qquad (5)$$

where the threshold T is chosen for the higher frequency RR intervals, which will allow the removal of ectopic beats whilst retaining the signal quality. Therefore coefficients above this threshold are set zero.
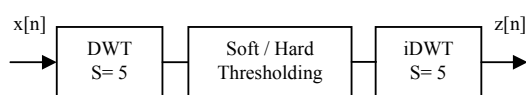

Fig. 3 Wavelet thresholding and filtering

The block diagram of Figure 3 outlines the process of filtering ectopic beats from RR interval signals using wavelet filtering. The instantaneous RR intervals are first passed through the DWT with up to 5 levels of decomposition (scales S=5) illustrated on the left side of Figure 2. Hard thresholding is applied to each wavelet coefficient for each scale or subband using Equation (5), where T is precomputed based on the average level of DWT coefficients produced from ectopic beats. Following hard thresholding the iDWT is applied to the coefficients where higher amplitude coefficients generated by ectopic beats are replaced with zero. The iDWT process is illustrated on the right side of Figure 2 showing the

reconstruction of the filtered signal. This filtering process has the effect of interpolating bad beats.

E. Interpolation

Another approach for removing ectopic beats is by interpolation. Ectopic beats are first identified by DWT and then 2 beat cycles are low pass interpolated to create a smooth signal. Ectopic beats are typically beats with a shorter cardiac cycle (coupling interval), followed by a longer cardiac cycle (post-extrasystolic pause). The ectopic beats are thus replaced by linear interpolated samples expressed in Equation (6)

$$X = \sum_{n=0}^{N-1} a_n x_N \qquad (6)$$

where N = 17 and the a terms are FIR filter coefficients modeling a symmetrical filter which allows the original data to pass through unchanged and interpolates between samples so as the mean square error between them and their ideal values is minimized. The sample outputs are the last samples in the 17 long sequence going back 9 cycles and placing zeros between each cycle to be interpolated.

F. Simulation

Before applying the detection and correction procedures to real signals a simulation was designed to be roughly representative of the characteristics of real life respiratory and heart rate signals. This enables simple testing of detection accuracy. Equations (7) and (8) simulate the RR interval and tidal volume signals respectively,

$$s(t) = A\sin(2\pi f_h t + \alpha_h) + B\sin(2\pi f_l t + \alpha_l) + C \qquad (7)$$

$$Vt(t) = D\cos(2\pi f_h t) + E \qquad (8)$$

where A is the peak-to-peak RSA amplitude per breath expressed in ms, B is the sympathovagal balance expressed as a ratio of LF to HF power and C is the mean RR interval. Tidal volume is expressed by D, and E is a DC offset whose value depends on ribcage and abdominal cross sectional area, which varies with changes in posture and mass, as the signals are DC coupled. The parasympathetic (HF) and sympathetic (LF) components have frequencies fh , fl and phases αh, αl respectively. The signals are sampled with 1ms resolution where t = 0, 0.001..299, for a 300 second or 5 minute duration. The instantaneous RR interval signal is thus derived from Equations (9) and (10).

$$RR(0) = s(0) = C \qquad (9)$$

$$RR(i) = s\left(1000\sum_{n=0}^{i-1} RR(n)\right) \qquad (10)$$

The sum of all previous RR intervals determines the time of the beat that is applied to Equation (11), where i is the beat number. Each sample is then repeated for the duration of the cycle length in 20ms sample intervals providing the 50 Hz sample rate expressed as follows:

$$RR_{cont}(k) = RR(i), \qquad k = i, 0.02....i+1 \qquad (11)$$

III. RESULTS

Each example presented uses Daubechies p = 4 wavelet filters. Higher orders were examined with each set having similar results. The first set of results presented is based on the heart rate simulation previously described. The output is illustrated in Figure 4 for a parameter set with high and low frequencies of 0.2 and 0.1 Hz respectively with no phase variation applied. A high frequency amplitude of A = 200 ms, B = 50% for a LF/HF ratio of 1/2 and C = 1000 ms is applied. Ectopic beats were inserted randomly where the RR interval would drop significantly indicating a high heart rate for one cycle, and increase significantly above the mean for one cycle. Figure 4 shows the RR interval sampled uniformly at 50Hz and decimated to 5Hz respectively for HRV spectral analysis. The following 2 signals illustrate the instantaneous RR interval followed by a set of wavelet coefficients from the highest frequency band. Figure 5 illustrates DWT coefficients for each band, where it is obvious band 1 effectively identifies ectopic beats.
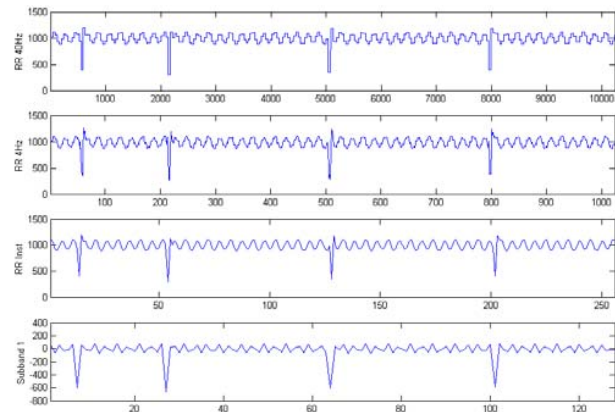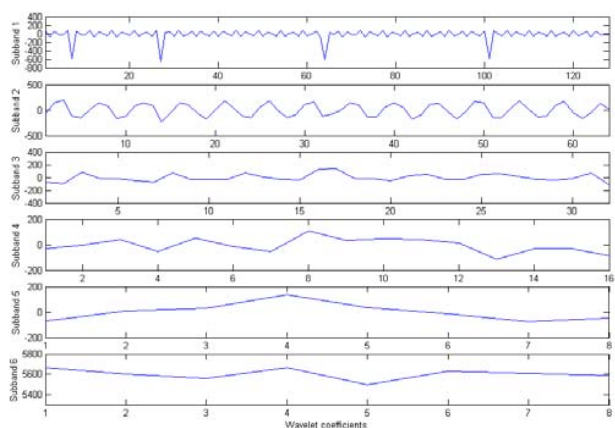

Fig. 4 Simulation with ectopic beats
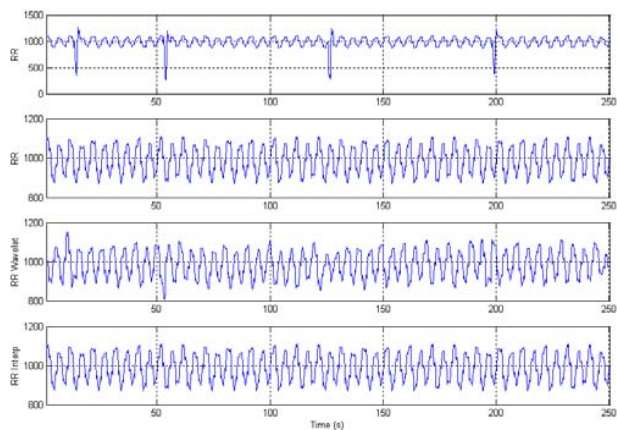

Fig. 5 Wavelet coefficients for 6 subbands

Fig. 6 Filtered and ectopic RR signals

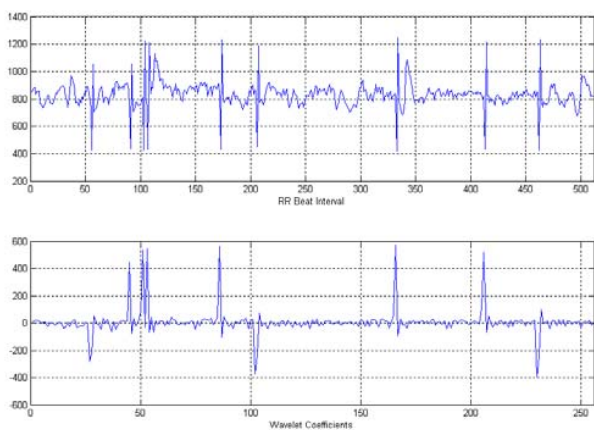Fig. 7 Frequency spectra of simulated signals

Fig. 8 RR signal with DWT coefficients
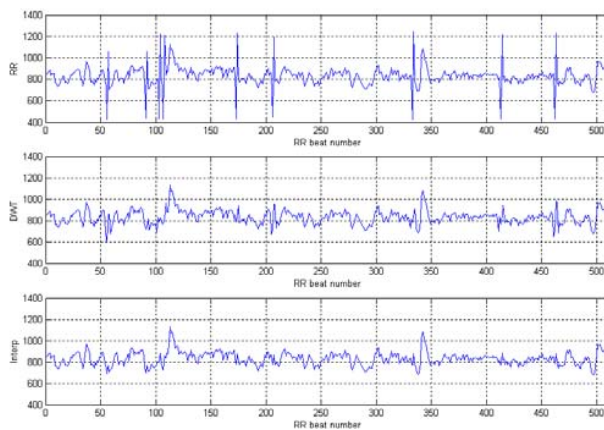
Fig. 9 RR signal with filtering and interpolation
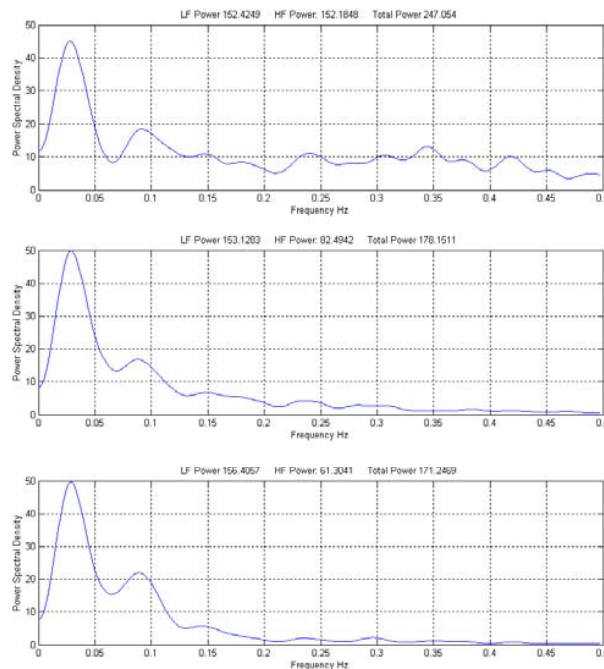
Fig.10 Frequency spectra of raw and filtered signals

The traces illustrated in Figure 6 include the RR interval signal with ectopic beats inserted, before insertion, DWT filtered and interpolated signals respectively. All signals resemble the simulation with no ectopic beats inserted. These signals were fed through the spectral analysis routine of section 3 with the results presented in Figure 7. The first spectral plot is the RR signal with no ectopic beats added. The second spectrum is that of the DWT filter and third the simulated RR signal with ectopic beats and no filtering. The interpolated signal is not presented as it perfectly replaces simulated data. The degrading effects of ectopic beats on power spectral analysis can be seen from the third trace where there exists spectral leakage across the complete spectrum. This has the effect of greatly increasing the power in each frequency band. For instance, the LF band has increased from 39.78 ms^2 to 100.2 ms^2 and the HF band has increased from 186.84 ms^2 to 249.5 ms^2. The second spectrum presented illustrates the ability of the DWT hard thresholding approach in removing these beats from the analysis. The power in LF band has increased from 39.78 to 46.17 ms^2. The HF band power has only increased by a negligible amount. A segment of heart rate data captured from the LifeShirt from a patient suffering from heart failure is illustrated 8. There exist 9
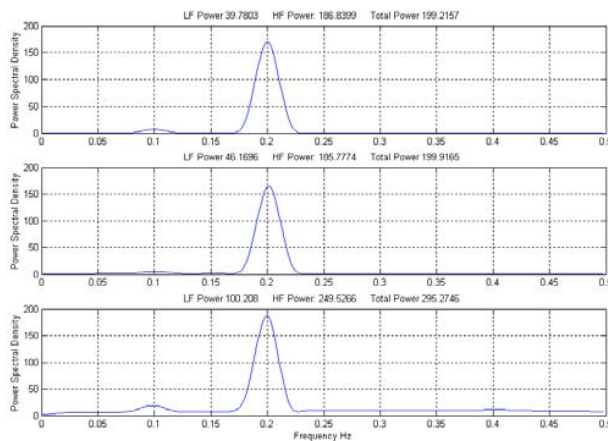
ectopic beats in this segment. Large negative or positive wavelet coefficients, several times in excess of the baseline identify each ectopic beat.

The first subband, which is the high frequency detailed level, is used to identify ectopic beats. As it is the first subband and the first level of decomposition, its length is half the RR segment length. The ectopic beats are thus identified as twice the largest coefficient index and the proceeding index.

The resultant signals from applying the linear interpolation algorithm, and the DWT thresholding approach are illustrated in Figure 9. It is clear both approaches have effectively filtered the appropriate beats. The resultant spectra from the filter outputs are shown in Figure 10. The first frequency spectrum is as expected with excessive spectral leakage created by the ectopic beats, and therefore the total spectral power is overestimated. The second spectrum demonstrates the output from the DWT threshold filter. As expected, the majority of spectral leakage is minimized, as is the total power. The third spectrum closely resembles that of the DWT with the exception that there is less power in the HF band. A more difficult signal to process is illustrated in Figure 11. 512 beats are shown with an average RR interval of approximately 600 ms. Furthermore the subject is ambulatory and there exists a non-stationary baseline. There exist 11 ectopic beats in this example which can all be clearly identified in the following trace where DWT coefficients of $\pm$ 50 of the previous beat is classified ectopic. These detected beats are filtered and interpolated with both techniques and illustrated in Figure 12. The two outputs look very similar where the DWT output has smoothed more beats. Whether or not the beats are ectopic is questionable, although would still impact spectral analysis somewhat. The spectra for each signal in Figure 12 are illustrated in Figure 13. The spectra in this case doesn't appear to have had as much spectral leakage introduced by ectopic beats as the previous examples. With closer examination of the power in each frequency band, the LF band power in each example is comparable. The spectral leakage power in the HF band of the interpolated approach appears to have attenuated the most noise.

IV. CONCLUSION

The examples presented show the accuracy of the DWT's ability to detect ectopic beats in the higher frequency subbands. This higher frequency component occurs as an ectopic beat generates a shorter cardiac cycle (coupling interval), followed by a longer cardiac cycle (post-extrasystolic pause). Therefore, this detection technique is robust throughout the population. Although the DWT hard thresholding approach appears to adequately filter the ectopic beats from the analysis, it does, in some circumstances alter the characteristic of the natural sinus rhythmic beats adjacent to it. Although this approach is much better than nothing at all, it does have an impact on the resultant spectrum. This approach is acceptable for displaying and time-domain measures, but problematic for spectral measures. Linear

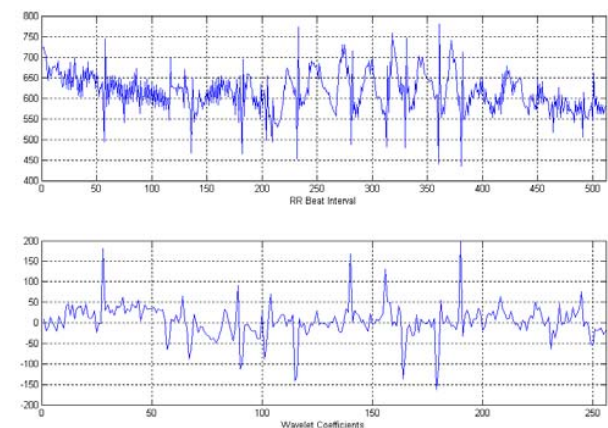interpolation has been shown to adequately replace the ectopic

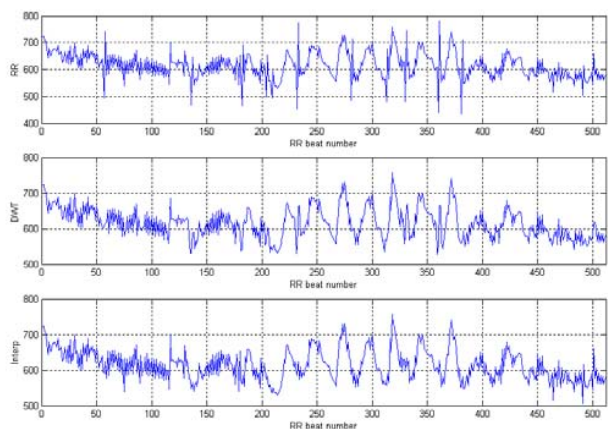Fig. 11 RR interval with DWT coefficients

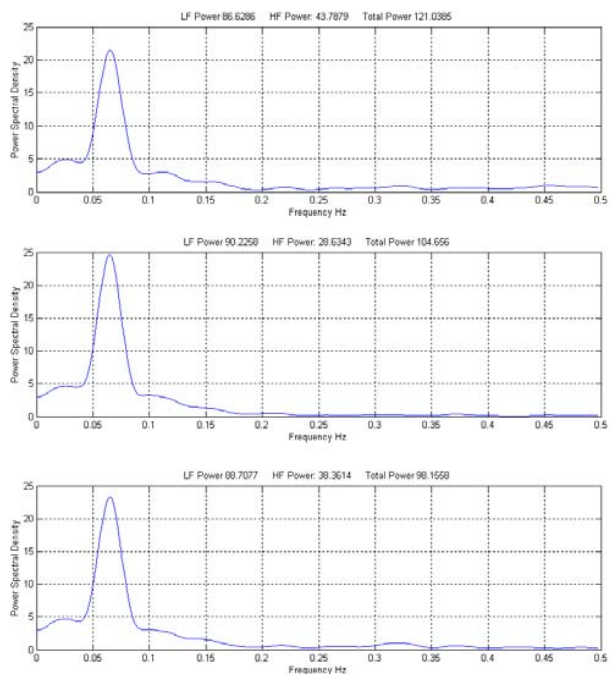Fig. 12 RR signal with filtering and interpolation

Fig. 13 Spectra of raw and filtered signals

beats with samples that can preserve the power spectrum. It is therefore concluded that the DWT detection algorithm with linear interpolation is a suitable automated combination for large datasets.

REFERENCES

[1] M. H. Crawford, S. Bernstein, P. Deedwania, "ACC/AHA guidelines for ambulatory electrocardiography," *Circulation*, vol. 100, pp. 886-893, 1999.

[2] N. Montano, T. Gnecchi Ruscone, A. Porta, F. Lombardi, M. Pagani, A. Malliani, "Power spectrum analysis of heart rate variability to assess the changes in sympathovagal balance during graded orthostatic tilt," *Circulation*, vol. 90, pp. 1826–1831, 1994.

[3] A. Malliani, M. Pagani, F. Lombardi, S. Cerruti, "Cardiovascular neural regulation explored in the frequency domain," *Circulation*, vol. 84, pp. 482–492, 1991.

[4] M. Pagani, N. Montano, A. Porta, "Relationship between spectral components of cardiovascular variabilities and direct measures of muscle sympathetic nerve activity in humans," *Circulation*, vol. 95, pp. 1441–1448, 1997.

[5] G. Paolisso, D. Manzella, N. Ferrara, et al. "Glucose Ingestion Affects Cardiac ANS in Healthy Subjects with Different Amounts of Body Fat," *American Journal of Physiology*, vol. 273, pp. E471–E478, 1997.

[6] A. Ravogli, G. Parati, E. Tortorici et al, "Early cardiovascular alterations in young obese subjects: evidence from 24-hour blood pressure and heart rate monitoring*," Europ. Heart J.*, vol. 98, pp. 3405A, 1998.

[7] R. M. Carney, J. A. Blumenthal, P. K. Stein, L. Watkins, D. Catellier, L. F. Berkman, S. M. Czajkowski, C. O'Connor, P. H. Stone, K. E. Freedland, "Depression, Heart Rate Variability, and Acute Myocardial Infarction," *Circulation*, vol. 104, no. 17, pp. 2024 – 2028, 2001.

[8] P. Grossman, J. A. Van Beek, "A Comparison of Three Quantification Methods for Estimation of Respiratory Sinus Arrhythmia," *Psychophysiology*, vol. 27, no. 6, pp. 702-714, 1990.

[9] K. Kotani, I. Hidaka, Y. Yamamoto, S. Ozono, "Analysis of Respiratory Sinus Arrhythmia with Respect to Respiratory Phase," *Methods of Information in Medicine*, vol. 39, pp. 153-156, 2000.

[10] J. Mateo, P. Gascón, L. Lasaosa, "Analysis of Heart Rate Variability in the Presence of Ectopic Beats Using the Heart Timing Signal," *IEEE Transactions on Biomedical Engineering*, vol. 50, no. 3, pp. 334-343, 2003.

[11] M. A. Murda'h,, W. J. McKenna, A. J. Camm, "Repolarization Alternans: Techniques, Mechanisms, and Cardiac Vulnerability," *Pacing Clinical Electrophysioly*, vol. 20, pp. 2641-2657, 1997.

[12] P. Laguna, R. Jané, P. Caminal, "Adaptive estimation of QRS complex by the Hermite model for classification and ectopic beat detection," *Medical and Biological Engineering and Computing*, vol. 34, pp. 58-68, 1996.

[13] M. A. Salo, T. Seppänen, H. V. Huikuri, "Ectopic Beats in Heart Rate Variability Analysis: Effects of Editing on Time and Frequency Domain Measures," *Annals of Noninvasive Electrocardiology*, vol. 6, no. 1, pp. 5-17, 2001.

[14] K. Konno and J. Mead, "Measurement of the separate volume changes of rib cage and abdomen during breathing," *J. Appl. Physiol.*, vol. 22, pp. 407-422, 1967.

[15] J. Sackner, A. Nixon, B. Davis, N. Atkins, and M. Sackner, "Non-invasive measurement of ventilation during exercise using a respiratory inductive plethysmograph. I," *Am. Rev. Respir. Dis.*, vol. 122, pp. 867-871, 1980.

[16] J. A. Adams, I. A. Zabaleta, D. Stroh, M. A. Sackner, "Measurement of breath amplitudes: comparison of three noninvasive respiratory monitors to integrated pneumotachograph," *Pediatr. Pulmonol.*, vol. 16, pp. 254-258, 1993.

[17] M. A. Sackner, and B. P. Krieger, "Non-invasive respiratory monitoring," In: Heart-Lung Interactions in Health and Disease, edited by S.M. Scharf, and S. S. Cassidy, New York: Marcel Dekker, pp. 663-805, 1989.

[18] M. A. Sackner et al, "Calibration of respiratory inductive plethyomograph during natural breathing," *J. Appl. Physiol.* vol. 66, pp. 410-420, 1989.

[19] M. A. Sackner et al, "Qualitative diagnostic calibration technique," *J. Appl. Physiol.*, vol. 87, 869-870, 1999.

[20] J. Pan and W. J. Tompkins, "A real-time QRS detection algorithm," *IEEE Trans. Biomed. Eng.*, vol. 32, no. 3, pp. 230-236, 1985..

[21] P. D. Welch, "The Use of Fast Fourier Transform for the Estimation of Power Spectra: A Method Based on Time Averaging Over Short, Modified Periodograms," *IEEE Trans. Audio Electroacoustics*, vol. AU-15, pp. 70-73, 1967.

[22] A. J. Camm, M. Malik, "Heart Rate Variability: Standards of Measurement, Physiological Interpretation and Clinical Use," Task Force of the Working Groups on Arrhythmias and Computers in Cardiology of the ESC and the North American Society of Pacing and Electrophysiology (NASPE). *European Heart Journal*, vol. 93, pp. 1043-1065, 1996.

[23] I. Daubechies, "Orthogonal bases of compactly supported wavelets," *Communications on Pure and Applied Mathematics*, vol. 41, pp. 909-996, 1988.

[24] D. L. Donoho, I. M. Johnstone, "Wavelet Shrinkage: Asymptopia?," *Journal of the Royal Statistical Societ*, Series B, vol. 57, pp. 301-369, 1995.

[25] D. L. Donoho, I. M. Johnstone, "Ideal time-frequency denoising, Technical Report," Department of Statistics, Standford University, 1994.

[26] D. L. Donoho, I. M. Johnstone, "Ideal Spatial Adaptation via Wavelet Shrinkage," *Biometrika*, vol. 81, pp. 425-455, 1994.

[27] D. L. Donoho, "De-noising by Soft Thresholding," *IEEE Transactions on Information Technology*, vol. 41, pp. 613-627, 1995.